Check for updates

Thermally Stable and Highly Conductive SAMs on Ag Substrate—The Impact of the Anchoring Group

Mateusz Wróbel, Tomasz Żaba, Eric Sauter, Mariusz Krawiec, Joanna Sobczuk, Andreas Terfort, Michael Zharnikov,* and Piotr Cyganik*

Self-assembled monolayers (SAMs) on metal substrates are an important part of modern interfacial chemistry and nanotechnology. The robustness of SAMs strongly depends on their thermal stability, which, together with electric conductivity, crucial for their applications in molecular/organic electronics. In this context, using a multidisciplinary approach, the structure, stability, and conductivity properties of conjugated aromatic SAMs featuring the naphthalene backbone and S—, Se—, or COO— group, mediating bonding to the Ag substrate are addressed. Whereas thermal stability of these SAMs exhibits a strong dependence on anchoring group, their conductivity is similar, which is rationalized by tentative model considering redistribution of charge density along the molecular framework. The thermal stability of model naphthalenethiol SAM, emphasized by desorption energy of ≈1.69 eV, is better than that of typical *N*-heterocyclic carbene (NHC) monolayers considered currently as the most stable SAMs on metal substrates. However, in contrast to NHC SAMs, which are highly insulating, the naphtalene-based SAM, with S—, Se— or COO— anchoring groups, are highly conductive, even in comparison with analogous oligophenyl SAMs (by a factor of 10). A unique combination of the ultimate thermal stability and superior conductivity for the naphthalenethiol SAM on Ag makes it highly attractive for applications.

1. Introduction

Self-assembled monolayers (SAMs) represent an important part of modern nanotechnology, building useful systems on their own and providing efficient means for modifications of surfaces and interfaces.[1] One of the primary functions of SAMs is the formation of well-defined, functional interfaces between organic and inorganic materials, which, to a large extent, are controlled by the properties of the chemical bonding formed between the SAM-building molecules and the substrate.[1a] The chemical and thermal stability and conductivity of such a SAM-engineered interface are the key parameters for most applications, including those in the areas of molecular/organic electronics and photovoltaics.[2] In all these areas, the need to optimize both thermal stability and conductance of SAMs is well justified by the mismatch between the vibrational density of states of the organic and inorganic materials. Due to this mismatch, thermal conductivity

---

M. Wróbel, T. Żaba, J. Sobczuk, Prof. P. Cyganik
Smoluchowski Institute of Physics
Jagiellonian University
Łojasiewicza 11
Krakow 30-348, Poland
E-mail: piotr.cyganik@uj.edu.pl

The ORCID identification number(s) for the author(s) of this article can be found under https://doi.org/10.1002/aelm.202000947.

[+]Present address: Institute of Functional Interfaces, Karlsruhe Institute of Technology (KIT), Hermann-von-Helmholtz-Platz 1, D-76344 Eggenstein-Leopoldshafen, Germany

Dr. E. Sauter[+], Prof. M. Zharnikov
Angewandte Physikalische Chemie
Universität Heidelberg
Im Neuenheimer Feld 253
Heidelberg 69120, Germany
E-mail: michael.zharnikov@pci.uni-heidelberg.de

Prof. M. Krawiec
Institute of Physics
Maria Curie-Sklodowska University
Pl. M. Curie Sklodowskiej 1
Lublin 20-031, Poland

Prof. A. Terfort
Institut für Anorganische und Analytische Chemie
Universität Frankfurt
Max-von-Laue-Straße 7
Frankfurt 60438, Germany

Prof. A. Terfort
School of Cyber Science
Nankai University
No.38 Tongyan Road
Jinnan District
Tianjin 300350, P. R. China

**ADVANCED
SCIENCE NEWS**
www.advancedsciencenews.com

**ADVANCED
ELECTRONIC
MATERIALS**
www.advelectronicmat.de

at the molecule–metal interface is rather low, which generally leads to overheating problems in the electric junctions based on such interface.[3] At the same time, it was demonstrated that the efficiency of the heat transport at the SAM-metal interface increases with the strength of bonding to the substrate and the packing density of the SAM.[3b, c] This observation was explained assuming that a stronger molecule–metal bonding makes the "spring constant" between organic film and inorganic substrate stiffer, which allows for more effective coupling of heat-carrying phonons across this interface.[3b,c] Thus, one can assume that densely packed and strongly bonded SAMs should be favorable for applications in the areas of molecular/organic electronics and organic photovoltaics.

Whereas the control of the molecular conductivity is doubtless crucial for molecular electronics and has been extensively analyzed in recent years,[4] the role of chemical and thermal stability of the molecule–metal interface was much less analyzed in the literature and their possible correlation with the conductivity still remains unclear. Specifically, dedicated brake-junction studies comparing different types of chemical bonding between individual molecules and Au electrodes, such as Au—N, Au—S, Au—P, and Au—C, indicated that increased strength of this bonding enhances the conductance of the junction.[5] In particular, an increase in conductance for the Au—C anchor as compared to the Au—S bond by one[5c] or even two[5b,d] orders of magnitude was reported, which could be correlated with the difference in the bond strength as estimated for the Au—S ($\approx$1.3 eV, on the basis of thermal desorption studies[6]) and Au—C bond ($\approx$3.0–3.5 eV, on the basis of density functional theory (DFT) calculations for alkanes[5b] and alkynes[7]). However, the better conductivity of the Au—C bond compared to Au—S was not confirmed by the large area molecular junction experiments[8] (based on eutectic GaIn) involving SAMs of alkanethiols and alkynes[9] on Au(111) substrate. These experiments revealed no difference in conductivity for these two types of SAMs.[8]

To address directly a possible correlation between the electric conductivity and the strength of molecule–metal bonding, two chemically and structurally analogous SAMs with naphthalene backbone, nitrile tailgroup, and either Au—S or Au—Se bonding to the substrate were analyzed, i.e., N≡C—C$_{10}$H$_6$—S(Se)/Au, abbreviated as NC-NapS(Se)/Au.[10] Series of experiments[10,11] and calculations[11b,c] for these and other SAMs demonstrated higher stability of the Au—Se bond compared to Au—S. However, the increase in the Au—Se bond stability was found to occur at the cost of lower stability of the adjacent Se—C bond compared to S—C,[10] which for SAMs with aliphatic backbone leads to positional oscillations in the stability of subsequent chemical bonds at the molecule–metal interface.[11c] The experiments conducted for NC-NapS(Se)/Au indicate that this effect is crucial both for thermal stability[11b] and conductivity[10] of SAMs. The higher stability of the Au—Se bond compared to Au—S in combination with lower stability of the Se—C bond compared to S—C leads to the overall lower thermal stability of selenium-based SAMs on Au, which is dictated not by the strongest but by the weakest (Se—C) link in the system.[11b] On the other hand, the conductivity analysis performed for NC-NapS(Se)/Au shows that modification of the bonding group from S to Se has no noticeable effect on charge transfer efficiency.[10] Since the tunneling process across SAMs involves

both Au—S(Se) and C—S(Se) bonds, it was supposed that strengthening of the former bond at the price of weakening of the latter causes a redistribution of the electron density at the Au—S(Se)—C interface, which, on the average, does not change the total probability of charge carrier tunneling.[10]

It would be important to verify whether the above considerations, formulated for thiols, and selenols on Au substrate, have a more general character and are valid for other types of SAMs as well. To this end, in the current study we take a step in this direction by dealing with Ag(111) substrate instead of Au(111) and by expanding the types of the anchoring group to carboxylic acid, which became increasingly popular recently in the context of molecular self-assembly.[12] Once again, we use intentionally SAMs with the naphthalene backbone and nitrile tail group, as schematically presented in **Figure 1**a, as they allow us to compare results of the current and former[10,11c,13] experiments and calculations, involving complementary techniques such as X-ray photoelectron spectroscopy (XPS), near-edge X-ray absorption fine structure (NEXAFS) spectroscopy, secondary ion mass spectrometry (SIMS), water contact angle (WCA) goniometry, conductivity measurements using-large area molecular junctions with liquid metal electrode (EGaIn), and calculations by using DFT. As to the selection of silver as the substrate, it is well justified by its highest conductivity among metals, better accessibility compared to gold which is the most commonly used material for electrodes in molecular electronics,[2a–c] and the very limited number of thermal stability studies[14] of SAMs formed on this substrate, with none of them addressing correlation of this parameter with the conductance. In addition, Ag electrodes are frequently used in molecular and organic electronics[15] and organic photovoltaics,[16] so that the results of the present study are directly relevant for these particular application areas.

2. Results and Discussion

The presentation and discussion of the experimental data is divided into three sections. The first section is related to the structural analysis of the SAMs, involving the XPS, NEXAFS spectroscopy, and WCA goniometry data. The next section deals with bonding to the substrate and thermal stability analysis relying on the SIMS, the TP-SIMS data, and DFT calculations respectively. The final part contains the electric conductivity analysis performed by using large-area molecular junctions with the top EGaIn electrode.

2.1. Structural Analysis (XPS, NEXAFS Spectroscopy, and WCA)

The XPS data are summarized in Figure 1b–f (additional data can be found in the Supporting Information; Figure S1). The S 2p spectrum of NC-NapS/Ag in Figure 1d can be fitted by a single S 2p$_{3/2,1/2}$ doublet at a BE of $\approx$162.0 eV (S 2p$_{3/2}$) which suggests the formation of well-defined Ag—S bonding for all SAM-building molecules with no traces of oxidized, unbounded, or atomic sulfur.[17] The respective analysis for the NC-NapSe/Ag was performed on the basis of the Se 3p spectrum (Figure 1e) which can be fitted by a single Se 3p$_{3/2,1/2}$ doublet at BE $\approx$161.0 eV (Se 2p$_{3/2}$). According to the established

**ADVANCED
SCIENCE NEWS**
www.advancedsciencenews.com

**ADVANCED
ELECTRONIC
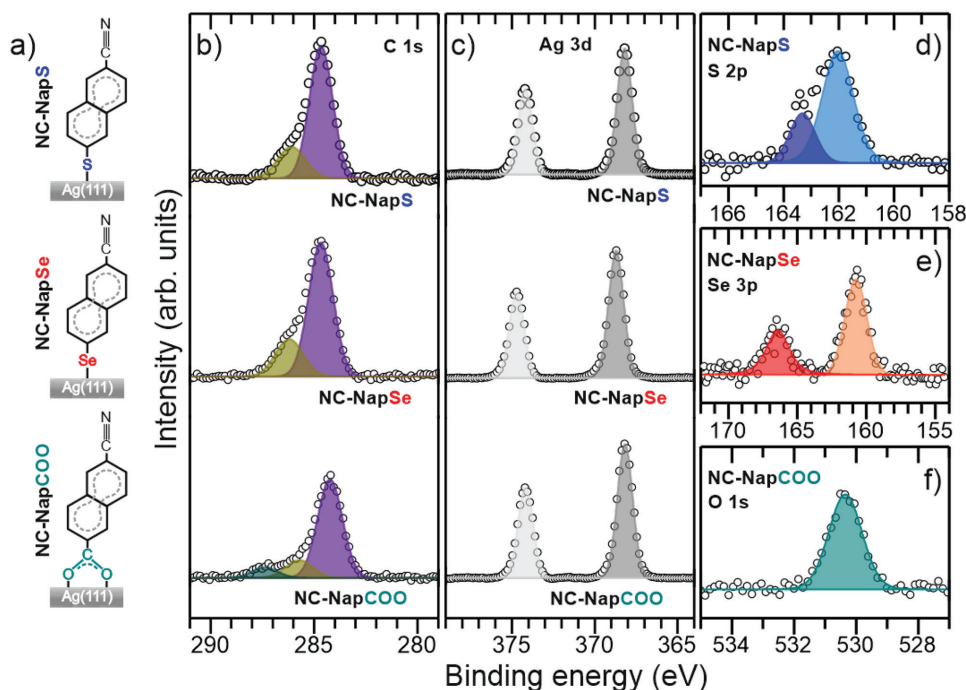MATERIALS**
www.advelectronicmat.de

Figure 1. Schematic representation of the SAM-forming molecules of this study adsorbed on Ag(111), along with their acronyms a) and XPS data b–f). The respective SAMs will be termed as NC-NapS/Ag, NC-NapSe/Ag, and NC-NapCOO/Ag or, in the case of Au(111) substrate, as NC-NapS/Au, NC-NapSe/Au. C 1s b) and Ag 3d c) XP spectra of NC-NapS/Ag, NC-NapSe/Ag, and NC-NapCOO/Ag; the S 2p d), Se 3p e), and O 1s f) XP spectra characteristic of the anchoring groups in NC-NapS/Ag, NC-NapSe/Ag, and NC-NapCOO/Ag, respectively. Individual peaks and components are marked using different colors (see text for details).

assignments[18] such a behavior suggests the formation of a well-defined Se−metal bond for all SAM-building molecules with no traces of oxidized or unbound selenium. The O 1s range for NC-NapCOO/Ag in Figure 1f can be fitted by a single and symmetric peak at BE ≈530.6 eV, which confirms the formation of well-defined bidentate carboxylate−Ag bond mediated by the COO− group.[12a,b,19]

The C 1s spectra of all samples are presented in Figure 1b with the dominant component indicated by violet color and assigned to the naphthalene backbone, in line with the literature data.[10,11b] For NC-NapS/Ag and NC-NapSe/Ag this component is located at a BE of ≈284.7 eV and for NC-NapCOO/Ag at a lower BE of ≈284.2 eV. Following the established analysis for analogous SAMs based on aromatic thiols and carboxylic acids[12a,b,20] this shift toward the lower BE by ≈0.5 eV can be attributed to the interfacial charge rearrangement. Such a collective electrostatic effect is most likely associated with the presence of an interfacial dipole layer[21] oriented toward the substrate as a result of Ag−O bond formation, which has an ionic character.[8,22] The same effect, even though less pronounced because of the low signal intensity, is also visible for the higher energy component (olive) assigned to the nitrile carbon,[23] which for NC-NapS/Ag and NC-NapSe/Ag is located at a BE of ≈286.1 eV but for NC-NapCOO/Ag at a BE of ≈285.7 eV exhibiting, thus, a similar BE shift (≈0.4 eV) as for the main peak. For NC-NapCOO/Ag, an additional and much less intense high energy component (dark green) was identified at a BE of ≈287.3 eV, which is characteristic of the COO− group involved in a bidentate Ag−carboxylate bond.[12a,b,19]

The Ag 3d signal presented in Figure 1c exhibits nearly equal intensity for all the samples, indicating similar film thicknesses, which has been evaluated using the standard approach based on the C 1s/Ag 3d intensity ratios,[24] assuming exponential attenuation of the photoelectron signal with the attenuation lengths reported earlier,[25] and using hexadecanethiol (HDT) SAMs on Ag as a reference system. As a result of this analysis, similar values of the effective film thickness of ≈1.25 and ≈1.31 nm were obtained for NC-NapS/Ag and NC-NapSe/Ag, respectively. For NC-NapCOO/Ag, a somewhat lower effective thickness value of ≈1.08 nm was estimated. We note at this point that lower effective film thickness for NC-NapCOO/Ag, compared to the monolayers with the S− and Se− docking groups, is also consistent with the more canted orientation of the molecules in these SAMs as concluded from the NEXAFS data (vide infra).

The C and N K-edge NEXAFS data for the SAMs of this study are presented in **Figure 2**a,b, accompanied by a schematic drawing of the molecular orientation in Figure 2c. Two types of spectra are shown, i.e., those acquired at an X-ray incidence angle of 55° (magic angle) and those corresponding to the difference between the spectra collected under the normal (90°) and grazing (20°) incidence geometry. These spectra provide complementary information. Specifically, the 55° spectra are representative of the electronic structure of the films (unoccupied molecular orbitals) and are not affected by orientational effects.[26] In contrast, the difference spectra represent fingerprints of orientational order and molecular orientation in a molecular film[26] expressed by the appearance of difference peaks at the positions of characteristic absorption resonances.
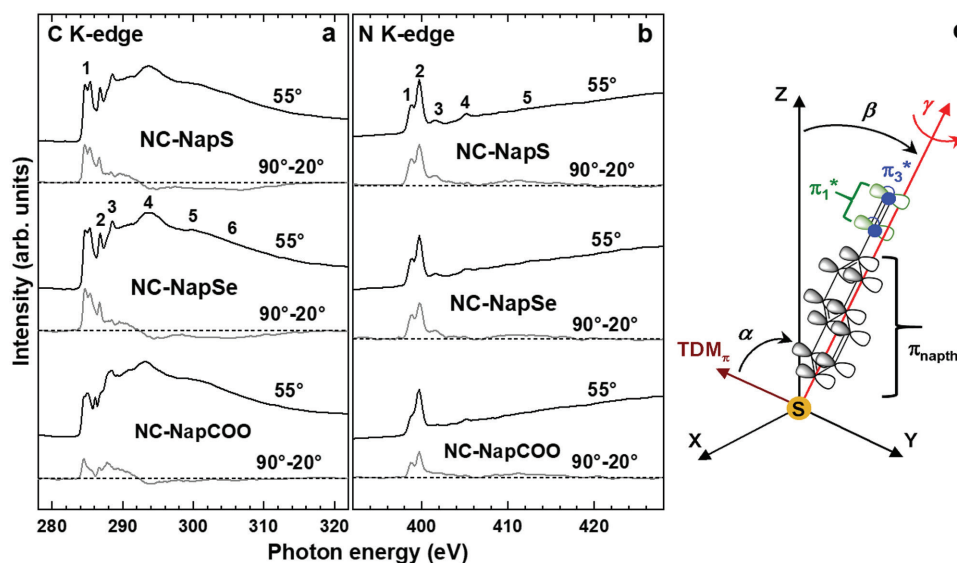
Figure 2. C a) and N b) K-edge NEXAFS spectra of NC-NapS/Ag, NC-NapSe/Ag, and NC-NapCOO/Ag acquired at an X-ray incidence angle of 55° (black lines), along with the respective difference between the spectra collected under the normal (90°), and grazing (20°) incidence geometry (gray lines). Individual absorption resonances are marked by numbers (see text for the assignments). The horizontal dashed lines correspond to zero. c) A schematic drawing of the orientation of the NC-NapS molecules in NC-NapS/Ag, representative of NC-NapSe/Ag, and NC-NapCOO/Ag as well. Molecular orientation is defined by the tilt and twist angles, β and γ, with the twist angle describing the rotation of molecule around its main axis (red arrow) and set to 0 if the π^* orbitals of the naphthalene backbone (π_{napth}^*; gray) are located in the tilt plane. The latter orbitals and the π_1^* orbital of the nitrile group (green) are parallel to each other and perpendicular to the backbone plane; the orientation of the respective transition dipole moment, (TDM$_\pi$, vine arrow) is given by the angle α. The π_3^* orbital of the nitrile group (blue) is parallel to the backbone plane.

The 55°C K-edge spectra of the SAMs of this study in Figure 2a exhibit characteristic resonances of the naphthalene backbone and the nitrile tail group, underlying the identity of the SAMs. The most representative feature of naphthalene is a double π^* resonance at 284.65 and 285.4 eV (**1a** and **1b**), with the characteristic intensity branching between the both components.[10] Such a double resonance is typical of acenes[27] and is usually associated with the chemical shift of the two symmetry-independent carbon atoms.[27b,28] The characteristic feature of benzonitrile is a sharp resonance at 286.7 eV (**2**).[10,29] Apart from these features, the spectra exhibit a π_2^* resonance at 288.5 eV (**3**), characteristic of the aromatic moieties,[26,28,30] and a variety of less specific σ^* resonances at higher photon energies. The relative intensities of individual features are nearly identical for NC-NapS/Ag and NC-NapSe/Ag, resulting in very similar spectral shapes, but somewhat different for NC-NapCOO/Ag, presumably because of the conjugation between the naphthalene backbone and the anchoring carboxyl group.

The N K-edge NEXAFS spectra of NC-NapS/Ag, NC-NapSe/Ag, and NC-NapCOO/Ag in Figure 2b exhibit the characteristic spectral features of benzonitrile, i.e., a strong, double π^* resonance at ≈398.8 and ≈399.7 eV (**1** and **2**), along with a weaker π^* resonance at ≈401.7 eV (**3**; presumably, π_4^* of nitrile)[31] and several hardly perceptible σ^* resonances at higher PEs (**4** and **5**). The most intense, double π^* resonance is representative of benzonitrile,[31,32] including monomolecular films containing such a building block.[10,29b,c,31b] This resonance stems from the conjugation between the π^* orbitals of the nitrile group and the adjacent phenyl ring lifting the degeneracy of the normally degenerated $\pi(C\equiv N^*)$

orbital.[31a,32] One of the resulting orbitals (**1**; π_1^*) becomes then oriented perpendicular to the plane of the adjacent ring (see Figure 2c) and strongly delocalized over the entire benzonitrile moiety. The other orbital (**2**; π_3^*) becomes oriented parallel to the plane of the adjacent ring (see Figure 2c) and is localized exclusively at the nitrile group. The delocalization of the π_1^* orbital leads to the lowered intensity of the respective absorption resonance, giving the characteristic branching of the entire π_1^*/π_3^* feature in the spectra.

Both C an N K-edge NEXAFS spectra of NC-NapS/Ag, NC-NapSe/Ag, and NC-NapCOO/Ag exhibit pronounced linear dichroism as follows from the presence of distinct peaks at the positions of the characteristic resonances in the 90°–20° difference spectra in Figure 2a,b. Considering that the transition dipole moments (TDMs) associated with the dominant π^* resonances are oriented perpendicular to the molecular axis, the positive sign of the respective difference peaks suggests, as expected, an upright orientation of the molecules in all three SAMs. Beyond this qualitative statement, quantitative evaluation of the entire sets of the C K-edge and N K-edge spectra was performed, relying on the standard theoretical framework for vector type molecular orbitals.[26,30b] As the result, the average tilt angles of the most prominent π^* orbitals of the naphthalene backbone (1a and 1b, see Figure 2a) and the nitrile moiety (π_1^* and π_3^*, see Figure 2b) were calculated. These angles, α_{napth}, α_1, and α_3, respectively, are compiled in **Table 1**.

Generally, for a nonsubstituted naphthalene backbone, only α_{napth} can be determined from the NEXAFS data and the calculation of the molecular tilt angle, β, according to equation[33]

$$\cos(\alpha_{napth}) = \sin(\beta) \times \cos(\gamma) \qquad (1)$$

Table 1. Average tilt angles of the π_{naphth}^*, π_1^*, and π_3^* orbitals derived from the numerical evaluation of the NEXAFS data for NC-NapS/Ag, NC-NapSe/Ag, and NC-NapCOO/Ag as well as the average molecular tilt and twist angles of the molecular backbone. The error bars are estimated at ±3°.

Average angles/system	NC-NapS/Ag	NC-NapSe/Ag	NC-NapCOO/Ag
π^* orbitals (naphthalene) – α_{naphth}	71	72°	65°
π_1^* orbital (N≡C) – α_1	78	75°	69°
π_3^* orbital (N≡C) – α_3	71	70°	64°
Twist angle (γ) from α_1 and α_3	38°	37°	37.5°
Molecular tilt (β) from α_1 and α_3	20°	17°	30°

will require the knowledge of the molecular twist angle, γ, which can be reasonably assumed based on the data for the respective bulk systems, determined by a complementary technique, such as infrared spectroscopy, or taken from theoretical simulations. However, in the present case, both β and γ can be directly determined from the NEXAFS data due to the intentional presence of the nitrile group, featuring the π_1^* and π_3^* orbitals, which are orthogonal to each other and aligned with the π^* system of the naphthalene backbone (see Figure 2c). Accordingly, using the α_1 and α_3 values, the average molecular tilt and twist angles can be directly calculated from the system of equations[29a]

$$\cos(\alpha_1) = \sin(\beta) \times \cos(\gamma) \qquad (2)$$

$$\cos(\alpha_3) = \sin(\beta) \times \cos(\pi/2 - \gamma) \qquad (3)$$

The derived β and γ values are compiled in Table 1. Accordingly, the molecular inclination in NC-NapS/Ag and NC-NapSe/Ag is small and similar, while that in NC-NapCOO/Ag is noticeably larger. At the same time, the average twist angles in all three SAMs are nearly identical, being larger than in the respective bulk material (25°)[34] but smaller than in NC-NapS(Se)/Au (52–54°).[10] Note that the monolayers on Au(111) are also characterized by much larger molecular inclination (42–43°),[10] which underlines the effect of the substrate and speaks for the higher quality of the SAMs on Ag(111).

The final step in the structural characterization of the naphthalene-based SAMs was probing the SAM-ambient interface by measuring advancing WCA. The respective parameter was evaluated at 62° ± 2°, 59° ± 3°, and 59° ± 2° for NC-NapS/Ag, NC-NapSe/Ag, and NC-NapCOO/Ag, respectively. Within the experimental error the above values are nearly identical to each other but differ by ≈10° from the analogous values reported earlier for NC-NapS(Se)/Au (≈50°).[10] This difference can be attributed to the somewhat different molecular orientation on Ag and Au substrates (as evident from the NEXAFS data) which should affect the WCA value. In any case, the observed WCA values correlate well with the expectations regarding the parameters of well-defined monolayers, terminated with the highly polar (≈3.6 D) [35] nitrile group.[36]

Summarizing this part, the structural analysis of NC-NapS/Ag, NC-NapSe/Ag, and NC-NapCOO/Ag indicates the formation of well-defined SAMs with similar thickness, molecular orientation, and SAM-ambient interface. Such similarity in the film structure suggests that the intermolecular interactions in these SAMs are also similar and, thus, the main contribution

to possible differences in their stability and electric conductivity can be directly attributed to the identity of the anchoring group (S−, Se−, and COO−) and the strength of its bonding to the substrate. Thus, the naphthalene-based monolayers of this study provide a suitable model system to test a possible correlation between the stability and electric conductivity in SAMs.

2.2. Stability Analysis (SIMS and TP-SIMS)

The SIMS spectra collected in the static mode for positive and negative secondary ions are presented in Figure S2 in the Supporting Information. For all analyzed samples, the spectra of both negative and positive secondary ions exhibit signals associated with the complete molecule (M), different molecular fragments, and molecule–metal clusters, such as MAg and M₂Ag. Whereas emission of the complete molecule directly identifies a monolayer, the emission of molecule–metal clusters is a well-known SIMS fingerprint of molecules chemisorbed on metal substrates.[13,37] To probe the stability of the molecule–metal bonding we were following the established methodology, applied previously to NC-NapS/Au and NC-NapSe/Au.[10] The data shown in **Figure 3**b represent the relative intensity of the [M–H]⁺, [M]⁺, and [M+H]⁺ signals, associated with the complete molecules (M). As schematically illustrated in Figure 3a, the emission of such ions is a consequence of breaking the chemical bond between the molecule and metal substrate triggered by the impact of the primary ions. The efficiency of this process depends both on the stability of the chemical bond, which has to be terminated to allow for emission, and the efficiency of ionization of the emitted fragment, which is presumably similar for NC-NapS and NC-NapSe.[10] As shown in Figure 3b, the intensity of the [M–H]⁺, [M]⁺, and [M+H]⁺ signals for NC-NapS/Ag is higher than that for NC-NapSe/Ag, which indicates higher stability of the Ag−Se bond compared to Ag−S in these SAMs. At the same time, this statement is fully consistent with analogous experiments conducted recently for a homologous series of hybrid, aromatic-aliphatic SAMs, $CH_3-(C_6H_4)_2-(CH_2)_n-S(Se)/Ag$ (BPnS(Se)/Ag; n = 2–6),[13] which underlines its general character for both aromatic and aliphatic SAMs on Ag(111). Following the same line of arguments, the lowest intensity of the [M–H]⁺, [M]⁺, and [M+H]⁺ signals observed for NC-NapCOO/Ag (Figure 3b) may indicate that bonding stability of these SAMs is even higher compared to NC-NapSe/Ag. As we discuss below, the interpretation of this type of data for the NC-NapCOO/Ag is not that straightforward.
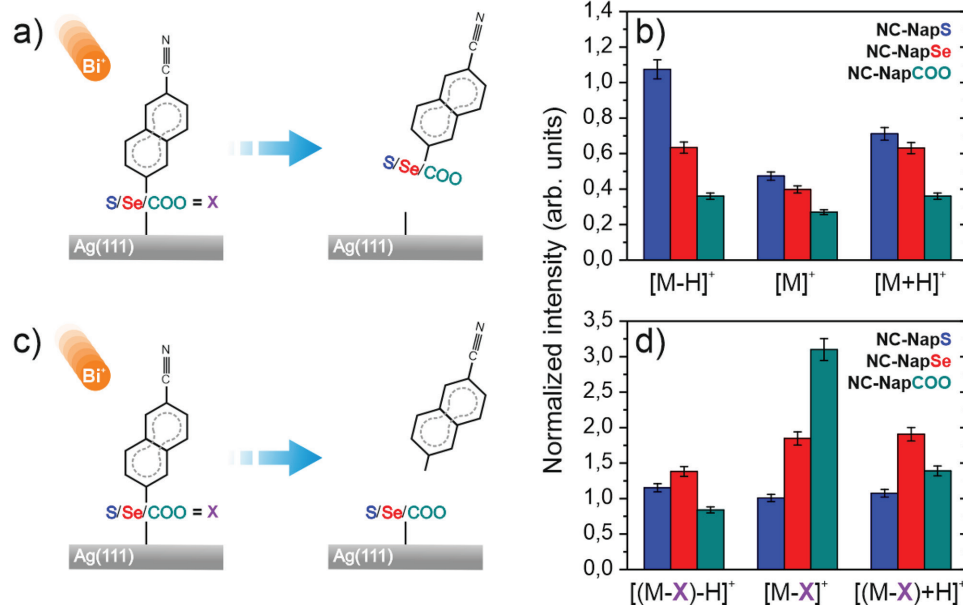
Figure 3. SIMS data analysis. Schematic drawings of bond scission between the anchoring group (S—, Se—, or COO—) and silver substrate a) or the rest of the molecule c). b) The intensity of the [M−H]+, [M]+, and [M+H]+ signals corresponding to the emission of the complete molecules for NC-NapS/Ag (blue bars), NC-NapSe/Ag (red bars), and NC-NapCOO/Ag (green bars). d) Analogous data for the emission of the molecules without anchoring group (which is denoted as X). The signals are normalized to the total intensity of the respective spectra. The error margins can be estimated at ±5%.

In the next step, we analyzed the emission of positive secondary ions related to the fragment without the bonding group, i.e., [(M−S/Se/COO)−H]+, [(M−S/Se/COO)]+, and [(M−S/Se/COO)+H]+ (Figure 3d). The release of these fragments requires the scission of the chemical bond between the anchoring group (S/Se/COO) and the adjacent carbon atom of the naphthalene backbone (as schematically indicated in Figure 3c). Comparing the intensities of the respective signals for NC-NapS/Ag and NC-NapSe/Ag (Figure 3d) we can conclude a higher stability of the S—C bond than that of Se—C. Thus, similar to the behavior of the analogous SAMs on Au(111),[10] stronger involvement of the Se anchoring group into the bonding with the Ag substrate compared to S, comes at the price of lower stability of the Se—C bond compared to S—C. Again, we note that this observation if fully consistent with the results of the analogous SIMS analysis conducted recently for the homologous BPnS(Se)/Ag series.[13]

In contrast, as shown in Figure 3d, the relative intensity of the [(M−COO)−H]+, [(M−COO)]+, and [(M−COO)+H]+ signals varies strongly depending on the type of the secondary ion, being either lower or higher than the analogous signals for NC-NapS/Ag and NC-NapSe/Ag. This observation indicates that the ionization probability for each of these fragments emitted from the NC-NapCOO/Ag is different from the analogous fragments emitted from NC-NapS(Se)/Ag. Therefore, in this particular case, the measured emission intensity cannot be used for estimating relative stability of the respective chemical bonds. In other words, as pointed also above, the correlation between the chemical bond stability and the efficiency in secondary ion emission is only possible for systems which have similar electronic structure to ensure similar ionization efficiency of the emitted fragments, as it is the case for the SAMs with Se— and S— anchoring groups. This observation also implies that the comparably small signal associated with the emission

of the complete molecule from NC-NapCOO/Ag, discussed above, cannot be attributed to the higher bonding stability of this system compared to NC-NapS(Se)/Ag. In fact, as will be discussed below, additional analysis indicates a higher stability of the Ag—S(Se) bond compared to Ag—carboxylate one.

Let us now discuss the thermal stability of the naphthalene-based SAMs. The analysis was conducted in situ by monitoring the SIMS signals upon the temperature ramping (3.75 K s−1) in the range from room temperature up to 700 K (TP-SIMS). Two types of secondary ions were simultaneously analyzed in these experiments, i.e., the [M]− signal (**Figure 4**a,b) corresponding to the emission of the complete molecules and the [AgX2]− signal (Figure 4c) related to the anchoring group (X = S, Se, O). To ensure that these signals were not affected by possible ion-induced damage of the sample, control measurements at room temperature were conducted exhibiting no change during the entire time needed for the data collection (see Figure S3 in the Supporting Information). The [M]− signal was used to monitor the surface coverage for the particular monolayer as a function of the sample temperature, to gain quantitative information such as desorption temperature (T_D), and desorption energy (E_D). The [AgX2]− signal was used as an additional source of qualitative information on the relative stability of the anchoring group bonding with the Ag substrate and with the rest of the molecule. To calculate the desorption temperature (T_D), the original [M]− data (Figure 4a), normalized to the values measured at room temperature, were differentiated as shown in Figure 4b. Accordingly, the T_D value depends strongly on the anchoring group with the highest, medium, and the lowest value for NC-NapS/Ag, NC-NapCOO/Ag, and NC-NapSe/Ag, respectively. The value of T_D for NC-NapS/Ag (≈555 K) is particularly high, suggesting surprisingly high thermal stability of this system compared to other types of SAMs formed on noble

**ADVANCED
SCIENCE NEWS**
www.advancedsciencenews.com

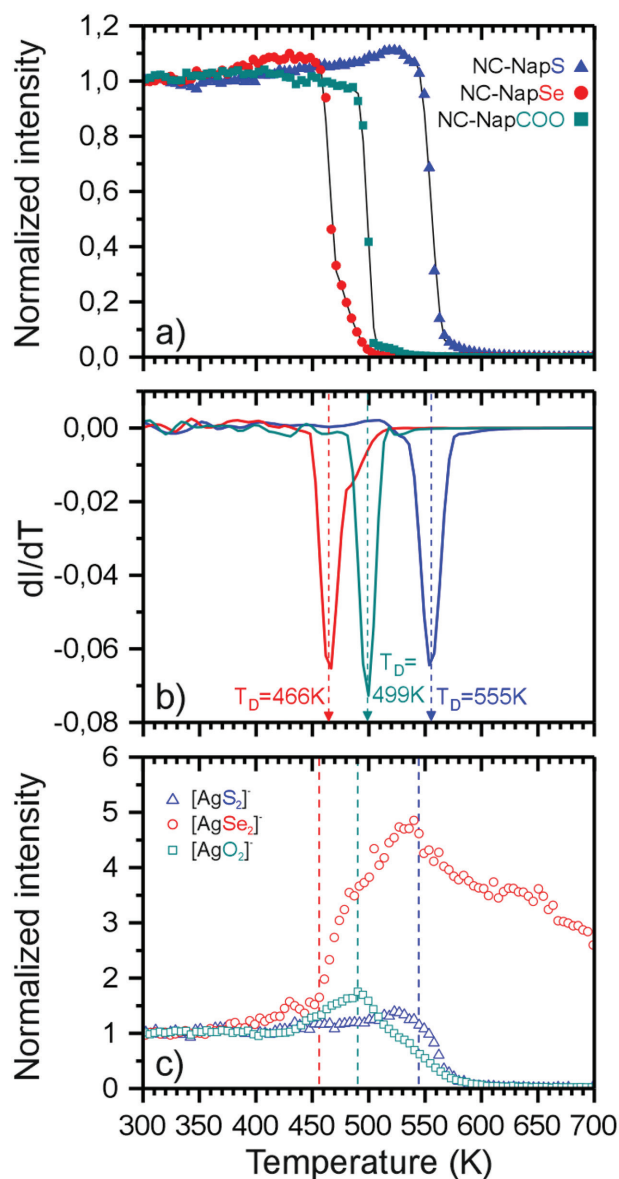**ADVANCED
ELECTRONIC
MATERIALS**
www.advelectronicmat.de

Figure 4. Thermal stability analysis using TP-SIMS. a) Normalized intensities (I) of the [M]⁻ signal for NC-NapS/Ag (blue triangles), NC-NapSe/Ag (red circles), and NC-NapCOO/Ag (green squares) as functions of the temperature. Black solid lines are spline functions fitted to the data points. b) Derivatives (dI/dT) of the aforementioned spline functions in a) for NC-NapS/Ag (blue line), NC-NapSe/Ag (red line), and NC-NapCOO/Ag (green line). The characteristic desorption temperatures (T_D) are indicated. In c) open symbols indicate the [AgX₂]⁻ (X = S, Se, O) signal for NC-NapS/Ag (blue triangles), NC-NapSe/Ag (red circles), and NC-NapCOO/Ag (green squares) as functions of the temperature. To correlate these signals with the monolayer desorption process, the corresponding onsets of a given desorption processes are indicated by the vertical dashed lines (the color code is analogous to the [AgX₂]⁻ data).

metal substrates and analyzed to date. However, considering the different rates of temperature ramping applied in former and current studies, which directly influence the observed T_D value, we calculate (using the Redhead formula[38] with a heating rate of 3.75 K min⁻¹ and a typical frequency factor of 10^{13} Hz used in most of previous SAM analysis[6,11b,39]) the

value of the desorption energy E_D of ≈1.69 eV, which can then be directly compared to other desorption experiments (taking the same value of the frequency factor in the Redhead formula). As a first system in this context, the basic alkanethiolate SAM, hexadecanethiol on Ag(111) (HDT/Ag) was tested (see Figure S4 in the Supporting Information). A T_D of ≈468 K obtained for HDT/Ag corresponds to E_D of ≈1.42 eV, which turned out to be in excellent agreement with the previous thermal desorption studies for alkanethiols on Ag substrate[14a] reporting E_D of ≈1.43 eV. Both ≈E_D values are noticeably lower than that for NC-NapS/Ag underlining the higher thermal stability of the latter system compared to typically used alkanethiols on the same substrate.

As a next step, NC-NapS/Ag can be compared to its analog on the Au substrate, i.e., NC-NapS/Au, for which a T_D of ≈448 K was measured at the same experimental conditions, corresponding to an E_D of ≈1.35 eV.[11b] Such a large difference in desorption energy for the thiols on these two substrates (≈0.34 eV) is surprising in view of the previous thermal desorption studies for alkanethiols on Au and Ag for which less different values of desorption energy were reported, i.e., ≈1.32[6] and ≈1.43 eV,[14a] respectively. Even more surprising is, however, the fact that the E_D value of ≈1.69 eV, obtained here for NC-NapS/Ag, is higher than the values reported for most of N-heterocyclic carbenes (NHC) SAMs on Au and Cu substrates, i.e., ≈1.64[39b] and ≈1.58 eV,[39c] respectively, which are currently considered[40] as probably the most thermally and chemically stable SAMs on noble metals. The only exception in this context is the very recent data obtained for highly-ordered NHC SAMs on Au substrate, for which a desorption energy of ≈1.89 eV was reported.[41] However, as we discuss in detail below, the NHC SAMs exhibit extremely low conductivity in contrast to the monolayers studied here.

Additional information on the thermal stability of the naphthalene-based SAMs is provided by the data presented in Figure 4c, where the onset of the desorption process, monitored by the [M]⁻ signal, is compared with the behavior of the [AgX₂]⁻ signal. For NC-NapS/Ag, the intensities of the [M]⁻ and [AgX₂]⁻ signals correlate with each other indicating that the desorption process involves mainly the removal of the complete molecules and, therefore, is controlled by the stability of the Ag—S rather than the S—C bond, with the former being the weakest link in this system, characterized by the desorption energy of ≈1.69 eV, derived in the present study.

As to NC-NapSe/Ag, the comparably low value of the E_D (≈1.41 eV) obtained here is most likely characteristic of the Se—C bond, which is the weakest link in the system. Such interpretation is consistent with the behavior shown in Figure 4c, where the onset of the desorption process, emphasized by the drop of the [M]⁻ signal, is accompanied by a rapid increase of the [AgSe₂]⁻ signal stemming from the Se atoms remaining on the substrate after the Se—C bond cleavage. We note at this point that whereas the [AgS₂]⁻ signal drops to zero level at ≈600 K indicating complete removal of S atoms from the Ag substrate, the [AgSe₂]⁻ signal intensity remains high even at 700 K, which hints toward a particularly strong bonding of the Se atoms to the Ag substrate, consistent with the formation of Ag₂Se alloys in this temperature range even at very low Se concentration,[42] in contrast to respective Ag₂S or Ag₂O compounds.[43]

ADVANCED
SCIENCE NEWS
www.advancedsciencenews.com

ADVANCED
ELECTRONIC
MATERIALS
www.advelectronicmat.de

The lower thermal stability of NC-NapSe/Ag compared to NC-NapS/Ag is also consistent with the lower stability of the Se—C bond compared to S—C as we concluded from the SIMS data. Consequently, we would like to stress again that increased involvement of the Se anchoring group compared to S into bonding with the metal substrate is achieved at the price of lowering stability of the subsequent chemical bond between the anchoring atom and the rest of the molecule which, importantly, is the weakest link of NC-NapSe/Ag, dictating their thermal stability.

As to NC-NapCOO/Ag, the bonding geometry in this case is more complicated with both oxygen atoms in the carboxylic group equally involved into the bidentate ionic bonding with the Ag substrate as concluded from our spectroscopic data. The correlation of the thermal and bonding stability at the molecule–metal interface is much more difficult to derive for this system considering the ambiguity in the interpretation of the static SIMS data pointed above. However, the TP-SIMS data presented in Figure 4c show that the onset of the monolayer desorption process, marked by the drop of the corresponding [M]⁻ signal, is accompanied by a drop of the [AgO₂]⁻ signal. Similar to NC-NapS/Ag, such a behavior indicates that thermal desorption of NC-NapCOO/Ag involves the removal of oxygen, and, therefore, is controlled by the stability of the Ag—carboxylate bond with the corresponding desorption energy of ≈1.52 eV. This value is lower than that for NC-NapS/Ag (≈~1.69 eV) indicating, thus, a lower stability of the Ag—carboxylate bond compared to Ag—S.

Summarizing this section, the bond stability analysis, conducted for NC-NapX/Ag (X = S, Se, COO) by a combination of SIMS and TP-SIMS experiments, indicates the following stability relations: 1) Ag—Se > Ag—S > Ag–carboxylate, 2) Ag—Se > Se—C, 3) Ag—S < S—C, 4) Ag–carboxylate < O—C (carboxylate), and 5) Ag–carboxylate < C—C (carboxylate–rest of the molecule). The weakest links in NC-NapS/Ag, NC-NapSe/Ag, and NC-NapCOO/Ag are the Ag—S, Se—C, and Ag—carboxylate bonds, corresponding to desorption energies of ≈1.69, ≈1.41, and ≈1.52 eV, respectively.

2.3. Stability Simulations (DFT)

Whereas the involvement of adatoms upon the adsorption of thiols is widely accepted for Au(111),[1d,44] their possible importance for Ag(111) is much less recognized,[45] providing a basis for one of our two models considered in current simulations, i.e., reconstructed Ag(111) surface with two adatoms per unit cell (another model is the flat, unreconstructed surface; see **Figure 5**). Considering, however, lack of experimental data regarding adatoms for carboxylic acid SAMs, we limited the current calculations to NC-NapS/Ag and NC-NapSe/Ag. To calculate the energies associated with breaking of Ag—S(Se) and S(Se)—C bonds we assumed that both SAMs form the same commensurate, high density, rectangular (3 × √3) structure with two molecules in the unit cell arranged in a herringbone pattern (see Figure 5). This structure mimics that of the analogous SAMs on Au(111)[11b] and is well justified by the film thicknesses and molecular tilt angles reported here. Even though tilt angles and the molecular twist are not reproduced by the simulations, the theoretical models of the molecular structure are expected to be good enough to monitor the energetics of the systems.

For the reconstructed Au(111) with two Au adatoms per (3 × √3) unit cell, previous studies indicated an adsorption structure of NC-NapS(Se) molecules in the form of an alternating chain of adatoms and anchoring atoms (S/Se), with each anchoring atom binding to two adatoms and each adatom binding to two anchoring atoms (see Figure 7 in ref [11b]). However, in the current analysis for Ag(111) surface, a different, but similar structure for S (Figure 5a–c) and Se (Figure S5a–c, Supporting Information) was found as a lowest energy configuration, where only one of two molecules in the unit cell binds to two adatoms while the other is bonded to one adatom and one surface atom (Figure 5a). The bond-breaking energies (as an averaged value for two molecules in the unit cell) for this structure and the structures obtained for the unreconstructed Ag(111) substrate are summarized in **Table 2**. Note, however, that in view of the complexity of the systems and a large
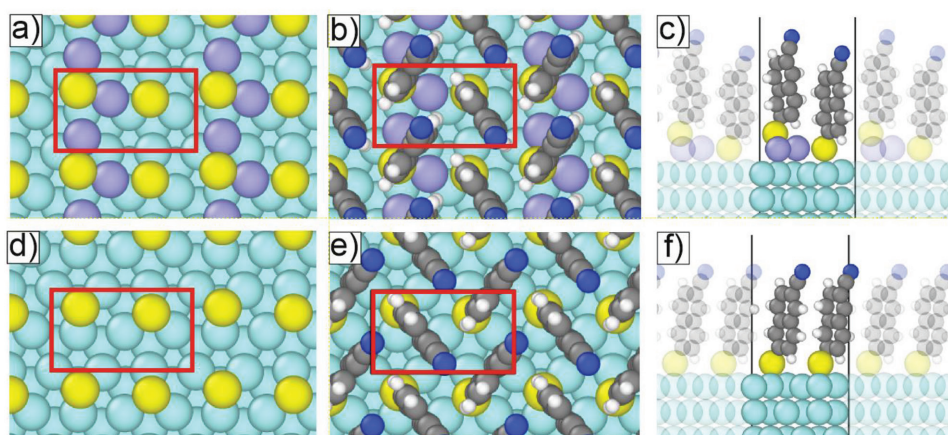

Figure 5. DFT simulations for NC-NapS/Ag. Top and side views of the NC-NapS adsorbed on adatom-decorated a–c) and adatom-free d–f) Ag(111) surface after geometry optimization. The rectangular (3 × √3) unit cells contain two molecules in herringbone arrangement and two a–c) or none d–f) Ag adatoms. In panels a) and d) only the docking groups and the Ag adatoms are displayed in order to show their relative positions. Different chemical species are marked by different colors: Ag—silver, Ag adatoms—purple, S—yellow, C—gray, H—white, and N—blue.

Table 2. Energetics of studied systems obtained from the DFT calculations: bond-breaking energies ($E_{X–Y}$, X = S or Se, Y = Ag or C) together with the order of the bonding energies.

Unit cell reconstruction	2 Adatoms				None			
Bond	Ag—S	Ag—Se	S—C	Se—C	Ag—S	Ag—Se	S—C	Se—C
$E_{X–Y}$ [eV]	2.870	2.947	3.039	2.701	2.631	2.673	3.181	2.855
	Order S—C > Ag—Se > Ag—S > Se—C				S—C > Se—C ≈ Ag—Se > Ag—S			

amount of the assumptions, including a temperature of 0 K in our simulations, these values should be taken as tentative only.

Keeping the above limitations in mind, we note as a first observation that for both anchoring groups (S and Se) the more efficient bonding to the metal substrate is obtained for the adatom-reconstructed surface than for the unreconstructed one, with slightly higher bonding energy for the Se case. Importantly, for both anchoring groups the increased strength of bonding to the reconstructed Ag(111) substrate is correlated with reduced strength of bonding between the anchoring group and the rest of the molecule. The same effect was suggested by the calculations for Au(111) substrate,[11b] confirming thus the general mechanism discussed above, in which increased involvement of the anchoring group into the bonding to the metal substrate is achieved at the price of lowering stability of the subsequent chemical bond between the anchoring atom and the rest of the molecule. As a next observation we point out that the S—C bond in NC-NapS/Ag is significantly stronger than S—Ag, which is fully consistent with the thermal stability experiments, and this effect is independent of the reconstruction of the Ag(111) substrate. In contrast, for the NC-NapSe/Ag system the change of the Ag(111) substrate from unreconstructed to reconstructed reverses the stability relation between the Se—C and Ag—Se bonds. Consequently, our calculations for NC-NapSe/Ag are only consistent with the experimental TPD data for the model assuming the involvement of the adatoms. In addition, comparing the stability of the Se—C (2.701 eV) and Ag—Se (2.947 eV) bonds within this model with the respective energies obtained for NC-NapS/Ag on unreconstructed (3.181 eV for S—C and 2.631 eV for Ag—S) and reconstructed (3.039 eV for S—C and 2.870 eV for S—Ag) substrate, the higher thermal stability of NC-NapS/Ag compared to NC-NapSe/Ag, defined by the lowest energy bond, is consistent with DFT calculations only for NC-NapS/Ag on reconstructed Ag(111) substrate (see bond stability order in Table 2). Thus, the DFT calculations not only confirm the analysis of molecule–metal interface stability based on the SIMS and TP-SIMS data, but also indicate the importance of the adatom adsorption model for NC-NapS/Ag and NC-NapSe/Ag.

2.4. Conductivity Analysis (EGaIn Measurements)

The final goal was the study of the electric transport properties of NC-Nap(S/Se/COO)/Ag in the large-area EGaIn junction,[46] which is currently one of the most commonly used approaches applied to this purpose.[2a] The top metal electrode in such a junction is formed by the eutectic GaIn liquid metal alloy which is covered by a spontaneously formed, thin (≈0.7 nm)

and conductive layer of Ga_2O_3.[15b] As schematically presented in **Figure 6**a, this layer forms a natural barrier for metal diffusion across the monolayer preventing short-cutting.[46] Due to its relatively simple design, the EGaIn method delivered a large amount of data for different types of SAMs such as thiolates,[46,47] carboxylates,[8,48] or alkynides.[8,49] The summary of the EGaIn junction data for NC-NapX/Ag (X = S, Se, COO) is presented in the top, middle, and bottom rows of Figure 6, respectively. Following the standard approach, verified by our own experiments, these data were obtained with a cone-shaped EGaIn electrode using flat Ag^{TS} substrates prepared by the template stripping (TS) method.[50] For all the samples, current density $J(V)$ [A cm^{-2}] measurements were conducted as a function of the applied voltage in the range from −0.5 to +0.5 V with the bottom Ag electrode (substrate) grounded. To acquire sufficiently large data statistics, ≈2000 $J(V)$ traces were collected for each analyzed system by forming ≈50 independent Ag^{TS}/SAM//Ga_2O_3/EGaIn junctions (here the "//" accounts for van der Waals contact between the SAM and Ga_2O_3 layer) and using 5 different samples for each type of the SAM (the exact numbers of traces are given in Figure 6).

The plots derived from the average of all traces obtained for NC-NapS/Ag, NC-NapSe/Ag, and NC-NapCOO/Ag are presented in Figure 6b,f,j, respectively, in the typically used, semilogarithmic fashion. To compare the conductivity of the SAMs studied here with the analogous values for other monolayers investigated by the same method, $\log|J(V)|$ values for −0.5 and +0.5 V are presented as histograms in Figure 6c,d,g,h,k,l for NC-NapS/Ag, NC-NapSe/Ag, and NC-NapCOO/Ag, respectively. All these histograms are nearly normally distributed and, therefore, could be fitted with the Gaussian function to calculate the corresponding mean values $\log|J(V)|$ and the standard deviations σ_{log}. To analyze the level of possible asymmetry of the $\log|J(V)|$ curves for +0.5 and −0.5 V bias voltages, the rectification factor, $r^+ = |J(+0.5)|/|J(−0.5)|$, was calculated from every measured $J(V)$ trace. The respective histograms of $\log|r^+|$ data were fitted with the Gaussian functions to determine the mean values $\log|r^+|$ and its standard deviations σ_{log} as shown in Figure 6e,i,m for NC-NapS/Ag, NC-NapSe/Ag, and NC-NapCOO/Ag, respectively.

Before discussion of the above results, we would like to point out that the level of statistics (≈2000 traces) presented here is noticeably higher than most of the EGaIn data sets published to date, with at the same time very narrow data distributions, which altogether confirms high quality and reproducibility of our measurements as well as reliability of the results. As a first observation, we note that the mean values of the $\log|J(+0.5 V)|$ obtained for NC-NapS/Ag (≈2.90), NC-NapSe/Ag (≈2.88), and NC-NapCOO/Ag (≈2.74) are nearly indistinguishable within the range of the respective standard deviations (σ_{log} 0.11–0.27). The mean values of $\log|J(−0.5 V)|$ exhibited similar behavior and were
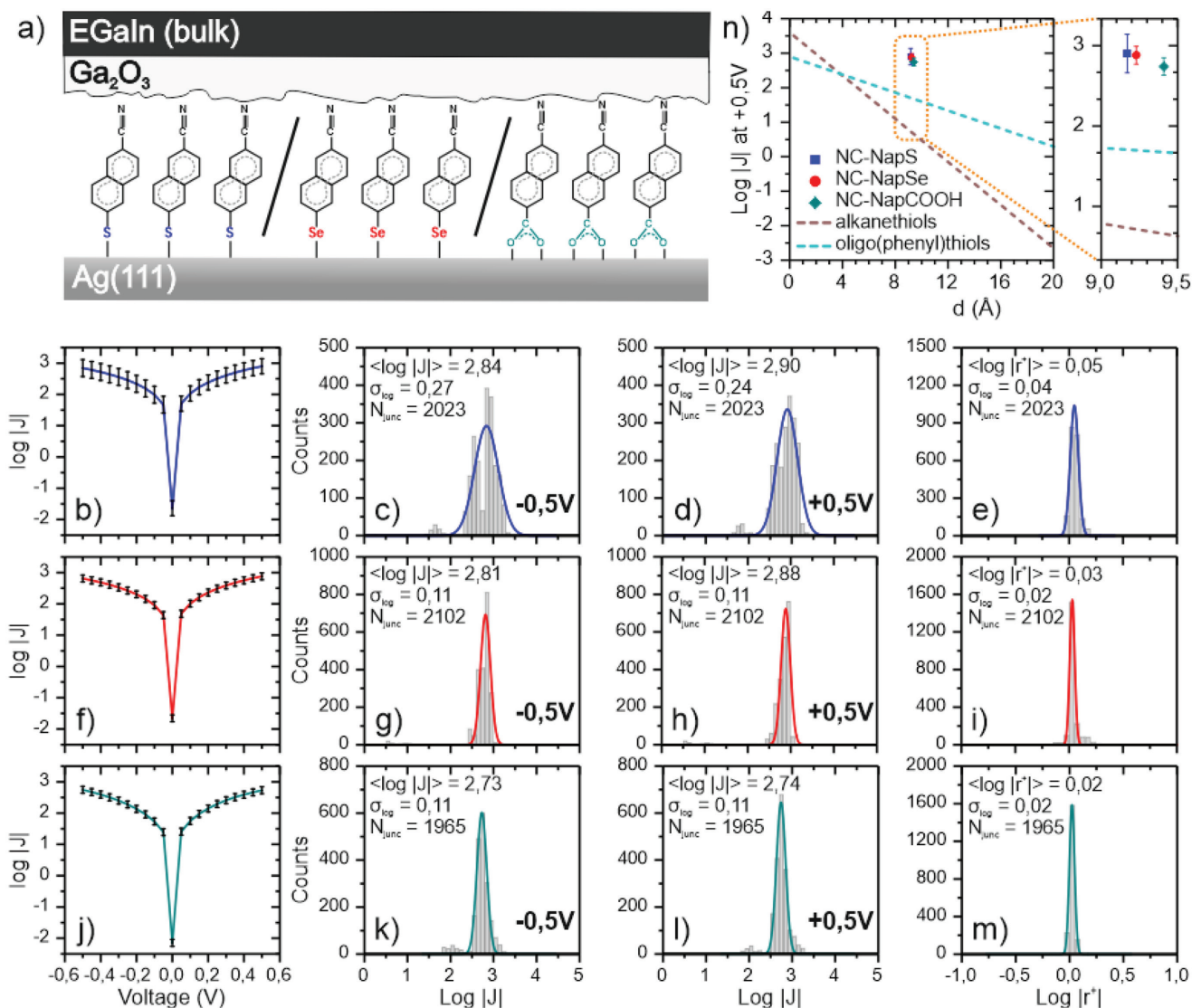
Figure 6. Electric conductivity analysis by EGaIn junctions measurements. a) Schematical drawing of the EGaIn junction. In (b), (f), and (j) log|$J(V)$| plots for NC-NapS/Ag, NC-NapSe/Ag, and NC-NapCOO/Ag, respectively, are presented. The error bars represent the standard deviation of the mean values. Histograms of log|$J(−0,5V)$| c,g,k), log|$J(+0,5V)$| d,h,l), and log|r^+| e,i,m) are presented for NC-NapS/Ag c,d,e), NC-NapSe/Ag g–i), and NC-NapCOO/Ag k–m). n) Comparison of the electric conductivity of NC-NapS/Ag, NC-NapSe/Ag, and NC-NapCOO/Ag with those of alkanethiols and oligophenylthiols on Ag(111). See text for details.

nearly identical to the above values, which results in the rectification factor (log|r^+| close to zero (within its standard deviation) as demonstrated by the respective histograms of this parameter shown in Figure 6e,i,m. Considering the significant dipole moment of the −CN group (3.6 D)[35] and theoretical models[51] indicating permanent dipole moment as a potential source of the rectification effect in thin organic films, one could probably expect a non-unity value of the rectification factor for the SAMs studied here. However, the recent systematic study[15c] of the dipole-moment-induced rectification in SAMs on Ag using the EGaIn junctions indicates that for dipole moment located relatively far from the Ag electrode (as it is the case here, with −CN being the tail group of the SAMs) and the voltage range limited to ±0.5 V, a very little if any rectification factor is expected—in full agreement with our data.

The transport properties of the naphthalene-based SAMs can be compared to those of alkanethiols[52] and oligophenylthiols[49a] on Ag substrate as shown in Figure 6n where the respective log|$J(+0.5 V)$| values are presented as functions of the molecule length d defined (as in the reference data) from the anchoring (S, Se, or O) to distal atom of the given system. The data for the reference SAMs are presented by the straight lines in accordance with the observed linear behavior following the simplified Simmons equation describing tunneling process

$$J = J_0 \cdot 10^{-\beta d/2.303} \tag{4}$$

with log|J_0| ≈ 3.7 and β ≈ 0.73 Å^{-1} for alkanethiols/Ag[51] and log|J_0| ≈ 3.0 and β ≈ 0.30 Å^{-1} for oligophenylthiols/Ag.[49a] As shown in Figure 6n and emphasized in the inset of this figure,

the current density of all three naphthalene-based SAMs is by more than an order of magnitude higher than that of the reference oligophenylthiol SAMs with the backbone of the same length *d*. Following former theoretical analysis,[53] we suppose that such a difference in the current density stems from a better conjugation of the naphthalene backbone compared to oligophenyls and the spreading of the relevant molecular orbitals over the entire molecule, including the anchoring group and the bond to the substrate.

The similar electric conductivity of NC-NapS/Ag and NC-NapSe/Ag mimics the behavior of NC-NapS/Au and NC-NapSe/Au, for which the dynamics of the charge transfer turned out to be independent of the anchoring group.[10] Such a behavior for both substrates can be correlated with the bond stability at the molecule–metal interface. Namely, according to the SIMS data, the higher strength of the Ag(Au)─Se bond compared to Ag(Au)─S is achieved at the price of lower stability of the subsequent Se─C bond compared to S─C. The tunneling process, responsible for the charge transfer across the SAMs, takes place through both Ag(Au)─S(Se) and S(Se)─C bonds. One can then reasonably assume that strengthening of the former bond accompanied by the weakening of the latter causes only a redistribution of the charge density within the Ag(Au)─S(Se)─C "linker" and, as the whole, does not change the total probability of the charge carrier tunneling. Considering that the S─ and Se─ docking groups are chemically similar, NC-NapS(Se)/Au(Ag) represent suitable model systems to verify the above hypothesis.

NC-NapCOO/Ag is an extension of these model systems to SAMs with chemically different bonding to the substrate (ionic instead of covalent) and different bonding geometry (bidentate instead of monodentate). Whereas the SIMS data do not allow an unequivocal conclusion regarding the charge redistribution for NC-NapCOO/Ag, bond stability oscillations accompanied by a redistribution of the charge density can nevertheless be assumed on the basis of our previous data for the BP*n*COO/Ag series where such a behavior was distinctly observed.[54] This redistribution minimizes the effect of the special character of COO─Ag bond, so that the conductivity of NC-NapCOO/Ag becomes similar to that of NC-NapS/Ag and NC-NapSe/Ag, as shown in Figure 6n. This simple, phenomenological model is consistent with the literature data for both aliphatic[8,52,55] and aromatic (oligophenyl)[49a] SAMs showing similar conductivity for different docking groups such as thiols, carboxylic acids, and alkynes, as well as, for different substrates, such as Au and Ag.

3. Conclusions

NC-NapS/Ag, NC-NapSe/Ag, and NC-NapCOO/Ag, featuring the same backbone and the tail group and differing by the docking group only, were studied in the context of their thermal stability and electric transport properties, looking for possible correlation between these parameters. Extensive spectroscopic analysis of these SAMs showed that they have a well-defined and similar structure, which allow us to attribute possible differences in their thermal stability and conductivity to the molecule–substrate interaction controlled by the anchoring group (S─, Se─, or COO─). The thermal stability analysis revealed that NC-NapS/Ag is the most stable system, emphasized by the desorption energy of ≈1.69 eV, which is not only higher than those for NC-NapSe/Ag (≈1.41 eV) and NC-NapCOO/Ag (≈1.52 eV) but even higher than the values reported for the most of monolayers based on NHC, considered currently as the most stable SAMs on noble metal substrates (≈1.64 for the Au and ≈1.58 eV for the Cu substrate). The analysis of the experimental data brings out that the thermal stability of a particular SAM is not necessarily defined by the anchoring bond strength but by the "weakest link" within the molecular framework, which was explicitly defined for all three SAMs studied. This conclusion was fully reproduced by the results of the dedicated DFT calculations indicating also the key role of Ag adatoms in controlling both the strength of bonding to the substrate and the "weakest link" in the system.

In contrast to the differences in the thermal stability, the conductivity of all analyzed SAMs was found to be nearly identical, and about an order of magnitude higher as compared to oligophenyl SAMs of the same thickness. The independence of the conductivity on the type of docking groups was explained by redistribution of the charge density between the adjacent bonds at the molecule–substrate interface, so that a stronger bond between the docking group and substrate is accompanied by a weaker bond between the docking group and backbone, with the entire effect on the charge transport efficiency being equalized.

The ultimate temperature stability and superior electric transport properties of NC-NapS/Ag makes this particular system highly attractive for applications in organic and molecular electronics and organic photovoltaics, as far as Ag electrodes are utilized and their engineering by SAMs is required. Although the most recent study demonstrated that highly-ordered NHC SAMs on Au can exhibit even higher thermal stability (desorption energy of ≈1.89 eV), these monolayers, based on specific Au─C bond formation, are highly insulating with conductance lower by more than 5 orders of magnitude compared to highly conductive NC-NapS/Ag system of the same length.[41] The high thermal stability extends the operation range of the respective devices, allowing to disregard their heating during the operation, including that imposed by external conditions. It also releases limitations during the assembly of devices, with the deposition and annealing steps frequently requiring high temperature. The superior electric transport properties of NC-NapS/Ag are also of advantage for metal electrode modification, warranting better charge transport through the organic–metal interface and decreasing the contact resistance. Finally, along with the NC-functionality, other dipolar groups can be used allowing efficient tuning of the work function at the interfaces involving Ag electrodes.[56]

4. Experimental Section

All experimental details are provided in the Supporting Information file.

Supporting Information

Supporting Information is available from the Wiley Online Library or from the author.

Conflict of Interest

The authors declare no conflict of interest.

Author contributions

M.W. performed the XPS, SIMS, TP-SIMS, WCA, and most of EGaIn experiments. T.Ż. designed and build the EGaIn experimental system, wrote software for EGaIn data analysis and conducted part of EGaIn experiments, E.S. and M.Z. performed synchrotron based measurements (NEXAFS/XPS), M.K. conducted all DFT calculations, J.S. wrote the software for the EGaIn system and conducted initial EGaIn experiments, A.T. provided the NC-NapS(Se) molecules. P.C. supervised the project and wrote the paper together with M.Z. in consultation with all the authors.

[1] a) J. C. Love, L. A. Estroff, J. K. Kriebel, R. G. Nuzzo, G. M. Whitesides, *Chem. Rev.* **2005**, *105*, 1103; b) J. J. Gooding, S. Ciampi, *Chem. Soc. Rev.* **2011**, *40*, 2704; c) R. K. Smith, P. A. Lewis, P. S. Weiss, *Prog. Surf. Sci.* **2004**, *75*, 1; d) C. Vericat, M. E. Vela, G. Benitez, P. Carro, R. C. Salvarezza, *Chem. Soc. Rev.* **2010**, *39*, 1805.

[2] a) A. Vilan, D. Aswal, D. Cahen, *Chem. Rev.* **2017**, *117*, 4248; b) A. Vilan, D. Cahen, *Chem. Rev.* **2017**, *117*, 4624; c) S. Casalini, C. A. Bortolotti, F. Leonardi, F. Biscarini, *Chem. Soc. Rev.* **2017**, *46*, 40; d) R. M. Metzger, *Nanoscale* **2018**, *10*, 10316.

[3] a) D. G. Cahill, P. V. Braun, G. Chen, D. R. Clarke, S. Fan, K. E. Goodson, P. Keblinski, W. P. King, G. D. Mahan, A. Majumdar, H. J. Maris, S. R. Philpot, E. Pop, L. Shi, *Appl. Phys. Rev.* **2014**, *1*, 011305; b) L. Zhang, L. Liu, *ACS Appl. Mater. Interfaces* **2017**, *9*, 28949; c) M. D. Losego, M. E. Grady, N. R. Sottos, D. G. Cahill, P. V. Braun, *Nat. Mater.* **2012**, *11*, 502.

[4] a) R. M. Metzger, *Chem. Rev.* **2015**, *115*, 5056; b) D. Xiang, X. Wang, C. Jia, T. Lee, X. Guo, *Chem. Rev.* **2016**, *116*, 4318; c) T. A. Su, M. Neupane, M. L. Steigerwald, L. Vankataraman, C. Nuckolls, *Nat. Rev. Mater.* **2016**, *1*, 16002.

[5] a) Y. S. Park, A. C. Whalley, M. Kamenetska, M. L. Steigerwald, M. S. Hybersten, C. Nuckolls, L. Venkataraman, *J. Am. Chem. Soc.* **2007**, *129*, 15768; b) Z. L. Cheng, R. Skouta, H. Vazquez, J. R. Widawsky, S. Schneebeli, W. Chen, M. S. Hybertsen, R. Breslow, L. Venkataraman, *Nat. Nanotechnol.* **2011**, *6*, 353; c) W. Hong, H. Li, S. X. Liu, Y. Fu, J. Li, V. Kaliginedi, S. Decurtins, T. Wandlowski, *J. Am. Chem. Soc.* **2012**, *134*, 19425; d) W. Chen, J. R. Widawsky, H. Vazquez, S. Schneebeli, M. S. Hybertsen, R. Breslow, L. Venkataraman, *J. Am. Chem. Soc.* **2011**, *133*, 17160.

[6] D. J. Lavrich, S. M. Wetterer, S. L. Bernasek, G. Scoles, *J. Phys. Chem. B* **1998**, *102*, 3456.

[7] a) M. J. Ford, R. C. Hoft, A. M. McDonagh, *J. Phys. Chem. B* **2005**, *109*, 20387; b) Q. Tang, D. Jing, *J. Phys. Chem. C* **2015**, *119*, 10804.

[8] C. M. Bowers, K. C. Liao, T. Zaba, D. Rappoport, M. Baghbanzadeh, B. Breiten, A. Krzykawska, P. Cyganik, G. M. Whitesides, *ACS Nano* **2015**, *9*, 1471.

[9] T. Zaba, A. Noworolska, C. M. Bowers, B. Breiten, G. M. Whitesides, P. Cyganik, *J. Am. Chem. Soc.* **2014**, *136*, 11918.

[10] J. Ossowski, T. Wächter, L. Silies, M. Kind, A. Noworolska, F. Blobner, D. Gnatek, J. Rysz, M. Bolte, P. Feulner, A. Terfort, P. Cyganik, M. Zharnikov, *ACS Nano* **2015**, *9*, 4508.

[11] a) K. Szelagowska-Kunstman, P. Cyganik, B. Schüpbach, A. Terfort, *Phys. Chem. Chem. Phys.* **2010**, *12*, 4400; b) J. Ossowski, G. Nascimbeni, T. Zaba, E. Verwüster, J. Rysz, A. Terfort, M. Zharnikov, E. Zojer, P. Cyganik, *J. Phys. Chem. C* **2017**, *121*, 28031; c) J. Ossowski, J. Rysz, M. Krawiec, D. Maciazek, Z. Postawa, A. Terfort, P. Cyganik, *Angew. Chem., Int. Ed.* **2015**, *54*, 1336.

[12] a) A. Krzykawska, J. Ossowski, T. Zaba, P. Cyganik, *Chem. Commun.* **2017**, *53*, 5748; b) A. Krzykawska, M. Szwed, J. Ossowski, P. Cyganik, *J. Phys. Chem. C* **2018**, *122*, 919; c) H. Aitchison, R. O. de la Morena, R. Peifer, S. Omar, H. Lu, S. M. Francis, M. Zharnikov, A. Grohmann, M. Buck, *Langmuir* **2018**, *34*, 9654; d) R. O. de la Morena, A. Asyuda, H. Lu, H. Aitchison, K. Turner, S. M. Francis, M. Zharnikov, M. Buck, *Phys. Chem. Chem. Phys.* **2020**, *22*, 4205.

[13] J. Ossowski, J. Rysz, A. Terfort, P. Cyganik, *J. Phys. Chem. C* **2017**, *121*, 459.

[14] a) L. M. Rodriguez, J. E. Gayone, E. A. Sanchez, O. Grizzi, *J. Phys. Chem. B* **2006**, *110*, 7095; b) E. Ito, H. Ito, T. Hayashi, M. Hara, J. Noh, *J. Phys. Chem. C* **2012**, *116*, 17586.

[15] a) C. A. Nijhuis, W. F. Reus, J. R. Barber, M. D. Dickey, G. M. Whitesides, *Nano Lett.* **2010**, *10*, 3611; b) C. S. S. Sangeeth, A. Wan, C. A. Nijhuis, *J. Am. Chem. Soc.* **2014**, *136*, 11134; c) M. Baghbanzadeh, L. Belding, L. Yuan, J. Park, M. H. Al-Sayah, C. M. Bowers, G. M. Whitesides, *J. Am. Chem. Soc.* **2019**, *141*, 8969; d) B. de Boer, A. Hadipour, M. M. Mandoc, T. van Woudenbergh, P. W. M. Blom, *Adv. Matter.* **2005**, *17*, 621; e) J. P. Hong, A. Y. Park, S. Lee, J. Kang, N. Shin, D. Y. Yoon, *Appl. Phys. Lett.* **2008**, *92*, 143311.

[16] a) Z. Liang, Q. Zhang, L. Jiang, G. Cao, *Energy Environ. Sci.* **2015**, *8*, 3442; b) B. Xu, Z. Zheng, K. Zhao, J. Hou, *Adv. Mater.* **2016**, *28*, 434; c) Q. Zhang, W.-T. Wang, C.-Y. Chi, T. Wächter, J.-W. Chen, C.-Y. Tsai, Y.-C. Huang, M. Zharnikov, Y. Tai, D.-J. Liaw, *Energy Environ. Sci.* **2018**, *11*, 682; d) C.-Y. Chi, C.-H. Shih, E. Sauter, S. K. Das, H.-T. Lien, S.-T. Chang, M. Zharnikov, Y. Tai, *J. Mater. Chem. A* **2018**, *6*, 6542.

[17] a) A. Shaporenko, M. Elbing, A. Blaszczyk, C. von Hänisch, M. Mayor, M. Zharnikov, *J. Phys. Chem. B* **2006**, *110*, 4307; b) S. Fischer, A. C. Papageorgiou, M. Marschall, J. Reichert, K. Diller, F. Klappenberger, F. Allegretti, A. Nefedov, C. Wöll, J. V. Barth, *J. Phys. Chem. C* **2012**, *116*, 20356.

[18] H. Kondoh, I. Nakai, A. Nambu, T. Ohta, T. Nakamura, R. Kimura, M. Matsumoto, *Chem. Phys. Lett.* **2001**, *350*, 466.

[19] a) H. Aitchison, H. Lu, S. W. L. Hogan, H. Früchtl, I. Cebula, M. Zharnikov, M. Buck, *Langmuir* **2016**, *32*, 9397; b) H. Aitchison, H. Lu, M. Zharnikov, M. Buck, *J. Phys. Chem. C* **2015**, *119*, 14114;

**ADVANCED
SCIENCE NEWS**

www.advancedsciencenews.com

**ADVANCED
ELECTRONIC
MATERIALS**

www.advelectronicmat.de

c) I. Cebula, H. Lu, M. Zharnikov, M. Buck, *Chem. Sci.* **2013**, *4*, 4455.

[20] C. Neumann, M. Szwed, M. Frey, Z. Tang, K. Kozieł, P. Cyganik, A. Turchanin, *ACS Appl. Mat. Interfaces* **2019**, *11*, 31176.

[21] T. Taucher, I. Hehn, O. T. Hofmann, M. Zharnikov, E. Zojer, *J. Phys. Chem. C* **2016**, *120*, 3428.

[22] Y. T. Tao, *J. Am. Chem. Soc.* **1993**, *115*, 4350.

[23] a) H. Hamoudi, P. Kao, A. Nefedov, D. L. Allara, M. Zharnikov, *Beilstein J. Nanotechnol.* **2012**, *3*, 12; b) N. Ballav, B. Schüpbach, S. Neppl, P. Feulner, A. Terfort, M. Zharnikov, *J. Phys. Chem. C* **2010**, *114*, 12719.

[24] O. Dannenberger, K. Weiss, H. J. Himmel, B. Jager, M. Buck, C. Wöll, *Thin Solid Films* **1997**, *307*, 183.

[25] C. L. A. Lamont, J. Wilkes, *Langmuir* **1999**, *15*, 2037.

[26] J. Stöhr, *NEXAFS Spectroscopy; Springer Series in Surface Sciences*, Springer, Berlin **2003**.

[27] a) M. B. Robin, I. Ishii, R. McLaren, A. P. Hitchcock, *J. Electron Spectr. Relat. Phenom.* **1988**, *47*, 53; b) H. Ågren, O. Vahtras, V. Carravetta, *Chem. Phys.* **1995**, *196*, 47; c) H. Oji, R. Mitsumoto, E. Ito, H. Ishii, Y. Ouchi, K. Seki, T. Yokoyama, T. Ohta, N. Kosugi, *J. Chem. Phys.* **1998**, *109*, 10409; d) C. Partes, C. Yildirim, S. Schuster, M. Kind, M. Zharnikov, A. Terfort, *Langmuir* **2016**, *32*, 11474; e) C. Partes, E. Sauter, M. Gärtner, M. Kind, A. Asyuda, M. Bolte, M. Zharnikov, A. Terfort, *J. Phys. Chem. C* **2019**, *123*, 20362.

[28] T. Yokoyama, K. Seki, I. Morisada, K. Edamatsu, T. Ohta, *Phys. Scr.* **1990**, *41*, 189.

[29] a) N. Ballav, B. Schüpbach, O. Dethloff, P. Feulner, A. Terfort, M. Zharnikov, *J. Am. Chem. Soc.* **2007**, *129*, 15416; b) H. Hamoudi, S. Neppl, P. Kao, B. Schüpbach, P. Feulner, A. Terfort, D. Allara, M. Zharnikov, *Phys. Rev. Lett.* **2011**, *107*, 027801; c) M. Zharnikov, *J. Electron Spectr. Relat. Phenom.* **2015**, *200*, 160.

[30] a) J. Horsley, J. Stöhr, A. P. Hitchcock, D. C. Newbury, A. L. Johnson, F. Sette, *J. Chem. Phys.* **1985**, *83*, 6099; b) S. Frey, V. Stadler, K. Heister, W. Eck, M. Zharnikov, M. Grunze, B. Zeysing, A. Terfort, *Langmuir* **2001**, *17*, 2408.

[31] a) S. Carniato, V. Ilakovac, J.-J. Gallet, E. Kukk, Y. Luo, *Phys. Rev. B* **2005**, *71*, 022511; b) T. Wächter, L. Weinhardt, A. Terfort, M. Zharnikov, *J. Phys. Chem. C* **2018**, *122*, 12534.

[32] S. Rangan, J.-J. Gallet, F. Bournel, S. Kubsky, K. Le Guen, G. Dufour, F. Rochet, F. Sirotti, S. Carniato, V. Ilakovac, *Phys. Rev. B* **2005**, *71*, 165318.

[33] H. T. Rong, S. Frey, Y. J. Yang, M. Zharnikov, M. Buck, M. Wühn, C. Wöll, G. Helmchen, *Langmuir* **2001**, *17*, 1582.

[34] C. P. Brock, J. D. Dunitz, *Acta Cryst.* **1990**, *B46*, 795.

[35] L. G. Wade, *Organic Chemistry*, Pearson, Upper Saddle River, NJ **2010**.

[36] S. Frey, A. Shaporenko, M. Zharnikov, P. Harder, D. L. Allara, *J. Phys. Chem. B* **2003**, *107*, 7716.

[37] a) B. Arezaki, A. Delcorte, P. Bertrand, *Appl. Surf. Sci.* **2004**, *122*, 231; b) B. Arezaki, A. Delcorte, B. J. Garrison, P. Bertrand, *J. Phys. Chem. B* **2006**, *110*, 6832; c) S. C. C. Wong, N. P. Lockyer, J. C. Vickerman, *Surf. Interface Anal.* **2005**, *37*, 721; d) H. Y. Nie, *Anal. Chem.* **2010**, *82*, 3371.

[38] P. A. Redhead, *Vacuum* **1962**, *12*, 203.

[39] a) D. Rading, R. Kersting, A. Benninghoven, *J. Vac. Sci. Technol. A* **2000**, *18*, 312; b) C. M. Crudden, J. H. Horton, M. R. Narouz, C. A. Smith, K. Munro, C. J. Baddeley, C. R. Larrea, B. Drevniok, B. Thanabalasingam, A. B. McLean, O. V. Zenkina, I. I. Erbalidze, Z. She, H. Kraatz, N. J. Mosey, L. N. Saunders, A. Yagi, *Nat. Commun.* **2016**, *7*, 12654; c) C. R. Larrea, C. J. Baddeley, M. R. Narouz, N. J. Mosey, J. H. Horton, C. M. Crudden, *ChemPhysChem* **2017**, *18*, 3536.

[40] C. A. Smith, M. R. Narouz, P. A. Lummis, I. Singh, A. Nazemi, C. H. Li, C. M. Crudden, *Chem. Rev.* **2019**, *119*, 4986.

[41] A. Krzykawska, M. Wróbel, K. Kozieł, P. Cyganik, *ACS Nano* **2020**, *14*, 6043.

[42] I. Karakaya, W. T. Thompson, *Bull. Alloy Phase Diagrams* **1990**, *11*, 266.

[43] a) R. C. Sharma, Y. A. Chang, *Bull. Alloy Phase Diagrrams* **1986**, *7*, 263; b) K. Tokumitsu, *Solid State Ion* **1997**, *101–103*, 25.

[44] a) H. Häkkinen, *Nat. Chem.* **2012**, *4*, 443; b) P. Maksymovych, O. Voznyy, D. B. Dougherty, D. C. Sorescu, J. T. Yates, *Prog. Surf. Sci.* **2010**, *85*, 206.

[45] a) M. Yu, S. M. Driver, D. P. Woodruff, *Langmuir* **2005**, *21*, 7285; b) M. Yu, D. P. Woodruff, N. Bovet, C. J. Satterley, K. Lovelock, R. G. Jones, V. Dhanak, *J. Phys. Chem. B* **2006**, *110*, 2164; c) D. Otalvaro, T. Veening, G. Brocks, *J. Phys. Chem. C* **2012**, *116*, 7826.

[46] R. C. Chiechi, E. A. Weiss, M. D. Dickey, G. M. Whitesides, *Angew. Chem., Int. Ed.* **2008**, *47*, 142.

[47] a) M. M. Thuo, W. F. Reus, C. A. Nijhuis, J. R. Barber, C. Kim, M. D. Schulz, G. M. Whitesides, *J. Am. Chem. Soc.* **2011**, *133*, 2962; b) M. Baghbanzadeh, C. M. Bowers, D. Rappoport, T. Zaba, M. Gonidec, M. H. Al-Sayah, P. Cyganik, A. Aspuru-Guzik, G. M. Whitesides, *Angew. Chem., Int. Ed.* **2015**, *127*, 14956; c) M. Baghbanzadeh, C. M. Bowers, D. Rappoport, T. Zaba, L. Yuan, K. Kang, K. C. Liao, M. Gonidec, P. Rothemund, P. Cyganik, A. Aspuru-Guzik, G. M. Whitesides, *J. Am. Chem. Soc.* **2017**, *139*, 7624.

[48] K. C. Liao, C. M. Bowers, H. J. Yoon, G. M. Whitesides, *J. Am. Chem. Soc.* **2015**, *137*, 3852.

[49] a) C. M. Bowers, D. Rappoport, M. Baghbanzadeh, F. C. Simeone, K. C. Liao, S. N. Semenov, T. Żaba, P. Cyganik, A. Aspuru-Guzik, G. M. Whitesides, *J. Phys. Chem. C* **2016**, *120*, 11331; b) D. Fracasso, S. Kumar, P. Rudolf, R. C. Chiechi, *RSC Adv.* **2014**, *4*, 56026.

[50] E. A. Weiss, G. K. Kaufman, J. K. Kriebel, Z. Li, R. Schalek, G. M. Whitesides, *Langmuir* **2007**, *23*, 9686.

[51] C. Krzeminski, C. Delerue, G. Allan, D. Vuillaume, R. M. Metzger, *Phys. Rev. B* **2001**, *64*, 085405.

[52] M. Baghbanzadeh, F. C. Simeone, C. M. Bowers, K. C. Liao, M. Thuo, M. Baghbanzadeh, M. S. Miller, T. B. Carmichael, G. M. Whitesides, *J. Am. Chem. Soc.* **2014**, *136*, 16919.

[53] R. Cohen, K. Stokbro, J. L. M. Martin, M. A. Ratner, *J. Phys. Chem. C* **2007**, *111*, 14893.

[54] M. Wróbel, J. Ossowski, M. Krawiec, K. Kozieł, P. Dąbczyński, P. Cyganik, *Phys. Chem. Chem. Phys.* **2019**, *21*, 13411.

[55] K. C. Liao, H. J. Yoon, C. M. Bowers, F. C. Simeone, G. M. Whitesides, *Angew. Chem., Int. Ed.* **2014**, *53*, 3889.

[56] A. Petritz, M. Krammer, E. Sauter, M. Gärtner, G. Nascimbeni, B. Schrode, A. Fian, H. Gold, A. Cojocaru, E. Karner-Petritz, R. Resel, A. Terfort, E. Zojer, M. Zharnikov, K. Zojer, B. Stadlober, *Adv. Funct. Mater.* **2018**, *28*, 1804462.

2000947 (13 of 13)